CrossMark

Evolution of the Corrosion Morphology on AZ31B Tracked Electrochemically and by In Situ Microscopy in Chloride-Containing Media

M.A. MELIA,[1,2,3] T.W. CAIN,[1] B.F. BRIGLIA,[1] J.R. SCULLY,[1] and J.M. FITZ-GERALD[1]

1.—Department of Materials Science and Engineering, School of Engineering and Applied Science, University of Virginia, Charlottesville, VA 22904, USA. 2.—e-mail: mam2wv@virginia.edu. 3.—e-mail: Michael.melia756@gmail.com

The evolution of open-circuit corrosion morphology as a function of immersion time for Mg alloy AZ31B in 0.6-M NaCl solution was investigated. Real-time optical microscopy accompanied by simultaneous electrochemical characterization was used to characterize the filiform corrosion (FFC) of AZ31B. Specifically, the behavior of propagating corrosion filaments on the metal surface was observed, and correlations among polarization resistance, filament propagation rates, open-circuit potential, and active coverage of local corrosion sites were revealed. Three distinct stages of corrosion were observed in 0.6-M NaCl. An initial passive region, during which a slow potential rise occurred (termed stage I), a second FFC region (termed stage II) with shallow penetrating, distinct filaments, and a final FFC region (termed stage III) with deeper penetrating filaments, aligned to form a linear front. The electrochemical properties of each stage are discussed, providing insights into the penetration rates and corrosion model.

INTRODUCTION

The application space for Mg alloys has intensified within the past 15 years, and during this time, the focus has been on corrosion, which is a volatile and rapid process.[1] Critical understanding of the corrosion behavior is needed so that precise predictions of both corrosion rates and geometry can be made. Although a complete understanding of the Mg corrosion process is still developing,[2–4] some researchers have sought to understand how the corrosion morphologies may impact the corrosion rates.[5–12] In an attempt to bring clarity to this area, the research presented here analyzed localized corrosion via simultaneous electrochemical measurements as a function of immersion time. This study was conducted on an engineering-relevant Mg alloy, AZ31B, primarily immersed in quiescent 0.6-M NaCl, a simulant for sea water.

Recent studies to examine the corrosion morphology of the Mg family of alloys have focused on the evolution of a "filamentous" corrosion morphology

observed in Cl^- containing solutions, termed "filiform corrosion" (FFC).[5–7,12–16] The FFC observed on Mg alloys is unique in that a coating is not required, it is not based on a differential aeration model, and it is observed when an alloy surface is exposed to full immersion conditions.[5,14,15,17] Through detailed studies of FFC for Mg alloys, researchers have reported that the filament propagation and associated morphologies are sensitive to grain structure, local composition, secondary phase distribution, and local solution chemistry.[9,16,18] These investigations of filament formation across pure Mg or alloy surfaces have used several techniques including scanning vibrating electrode technique (SVET), time lapse optical microscopy, transmission electron microscopy (TEM), scanning electron microscopy (SEM), and electrochemical impedance spectroscopy (EIS).[5,8,10,13,14,18]

This article investigates the propagation of FFC, highlighting the resultant morphology and electrochemistry on the surface of AZ31B-H24 when immersed in chloride-containing solutions. Several trends between the electrochemical measurements

Evolution of the Corrosion Morphology on AZ31B Tracked Electrochemically and by In Situ
Microscopy in Chloride-Containing Media

2323

and time-dependent corrosion morphologies are revealed. Real-time video was used to show filament propagation, providing unique insights into H_2 evolution and the impact of changing corrosion morphology. The ramifications of local corrosion on corrosion rate are discussed using time-dependent EIS coinciding with the filament propagation videos. This article also reveals the distinct ability for filaments to propagate during specific stages of corrosion without any clear evidence of H_2 evolution in proximity to the propagating filament.

EXPERIMENTAL

AZ31B in the strain-hardened and partially annealed H24 condition with a grain size of approximately 6 μm (measured using the linear intercept technique). The as-received material is a Mg-Al-Zn alloy (3 wt.% Al, 1 wt.% Zn, 0.6 wt.% Mn, and 95.4 wt.% Mg) and its microstructure is presented in the supplemental data. Prior to corrosion testing, specimens were ground to a 1200-grit finish using Buehler® SiC paper in a Struers ethanol-based lubricant, free of water, to minimize surface oxidation. A colloidal silica finish was achieved for specimens used in optical corrosion videography. All tests were started within 30 min of the grinding or polishing process.

Corrosion experiments were performed in a quiescent 0.6-M NaCl solution, prepared the day of the experiments. Electrochemical measurements were performed in a standard three-electrode setup with the ground specimen as the working electrode, Pt mesh as the counter electrode, and a saturated calomel electrode (SCE) used as the reference electrode. Electrochemical measurements were conducted using electrochemical impedance spectroscopy (EIS) performed at the open-circuit potential (OCP). An area of 1 cm^2 was exposed to 250 mL of solution for the OCP/EIS measurements. EIS measurements were taken at immersion times dictated by the OCP and resulting morphology, typically at 5 min (prior to breakdown of passivity), 30 min (after breakdown), and successively at 60/120/240/360/720/1080/1440 min. The EIS measurements were performed over a frequency range of 100,000 Hz to 0.005 Hz at 6 points per decade using an amplitude of $\pm$ 10 mV. EIS data were analyzed, and a global polarization resistance (R_p) was determined using the equivalent circuit model and fitting procedure as described in previous work.[19–22] A large value of global R_p signifies a low corrosion current density $\left(i \propto \frac{1}{R_p}\right)$, where the R_p has been shown to be the dominating term in Stern-Geary determined Mg alloy corrosion rates.[19] In addition, an estimate for the R_p of a single filament in stages II and III is possible by conversion of the linear rate of propagation of metal corroded per second (or filament propagation rate, r (cm/s)) determined for each stage. Faraday's law was used in the form of:

$$i\left(\frac{A}{cm^2}\right) = r\left(\frac{cm}{s}\right) \times \left(\frac{AW\left(\frac{g}{mol}\right)}{n\left(\frac{eq}{mol}\right) \times F\left(\frac{C}{eq}\right) \times \rho\left(\frac{g}{cm^3}\right)}\right)^{-1}$$

Hence, a current density for a single FFC may be determined from optical microscopy where AW is atomic weight, n is the charge number that indicates electrons exchanged within a dissolution reaction, F is Faraday's constant, and ρ is the density of Mg. Using the Stern-Geary expression and assuming $B = 0.036$ V, the resistance of a single filament or corroding front, R_{FFC} (Ω-cm^2), can be determined by the corrosion current density in A/cm^2:[19,20]

$$R_{FFC}(\Omega \text{ - } cm^2) = \frac{B(V)}{i\left(\frac{A}{cm^2}\right)}.$$

Observations of the corrosion process were performed with a Dinolite^{TM} digital microscope for macroscopic images and with a Nikon® Optiphot-100 optical microscope for higher magnification. Real-time videos of the corrosion process on the optical microscope were captured with an AmScope MU-1000 CMOS camera. *ImageJ* was used to determine FFC propagation rates across the surface and the filament width. After immersion, samples were rinsed with DI water and cleaned via chromic acid (200-g/L CrO_3) per ASTM G-1 to remove the specimen corrosion products.[23] A Zygo® white light interferometer was used to measure filament depths. The combination of these techniques allowed for corrosion rate determination based on filiform areas, depths, and propagation behavior. All experiments and measurements were replicated a minimum of four times.

RESULTS AND DISCUSSION

Evolution of Electrochemical Behavior of AZ31B at OCP

The OCP, percent coverage of black filiform corrosion product, and global R_p measured by EIS are plotted as a function of immersion time in Fig. 1a. The OCP, which is close to -1.7 V_{SCE}, increases quickly to a peak at -1.57 V_{SCE} within the first 10 min, termed stage I.* Stage I signifies an incubation time required prior to initiation of localized corrosion on a nominally passive Mg surface. The global R_p measured by EIS of stage I was observed to be $\sim$900 Ω-cm^2, with the impedance spectra indicating two distinct capacitive loops (all impedance spectra are presented in supplemental data) and no signs of inductive behavior.[10,19,20,24] This suggests that corrosion of the partially passive native oxide dominates the initial electrochemical

---

*The use of the terms for each regime of FFC, stages I, II, and III, was adopted from Krebs et al.[13]
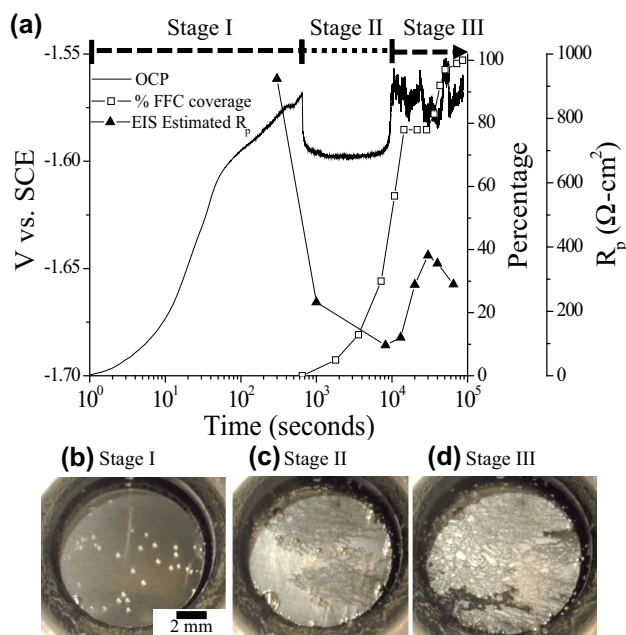
Fig. 1. One set of representative data for the OCP, percent coverage of filiform corrosion product, and EIS estimated global R_p plotted versus time of the AZ31B-H24 alloy immersed in 0.6-M NaCl is shown in (a). Representative optical images of the different corrosion stages occurring on AZ31B with time are shown in (b) to (d), correlated back with the plot in (a).

response for Mg alloys. Stage I corrosion is shown via the macroscopic time lapse image in Fig. 1b. In this image, large, stable bubbles of H_2 are observed on the surface. Typically the bubbles are attached to randomly distributed constituent Al-Mn intermetallic particles (IMPs) on the order of 5 μm in size found throughout the AZ31B microstructure. The gas bubbles are then observed to decrease in size and evolve as streams of H_2 upon breakdown of the oxide, signifying the initiation of local FFC.

Breakdown of the native oxide film typically occurred after ~10 min of immersion and initiated near one of the large Al-Mn IMPs, as observed in previous work.[8] This regime of corrosion, termed stage II, is characterized by a stable OCP that developed at -1.59 V_{SCE} (Fig. 1a) and the initiation of thin, individual corrosion filaments that propagate across the surface (Fig. 1c). During stage II, the global R_p measured by EIS was observed directly after the initiation of FFC. The resistance decreased in magnitude to ~200 Ω-cm^2 after 1000 s and continued to decrease in magnitude throughout the duration of stage II, reaching a local minimum, indicating a faster dissolution rate with time. After completion of stage II, the OCP increased to an average of -1.57 V_{SCE} with severe fluctuations in potential.

The rate of corrosion product coverage was observed to slow at the end of stage II with a black corrosion product covering ~78% of the surface (Fig. 1a). Complete coverage of the 1-cm^2 exposed surface with a dark corrosion product was observed

after ~24 h of immersion. In general, complete coverage by dark corroded regions is assumed when stage II is completed; nevertheless, silvery regions persist in between the shallow penetrating filaments.[10,14] The α-Mg, not yet affected by FFC, remains silver in color and has developed a thin, relatively uniform corrosion product at this stage made of MgO and Mg(OH)$_2$.[5,25–27] The black corrosion product is where deep localized corrosion occurs; hence, complete coverage of the surface by the localized corrosion morphology should be distinguished from the still, silvery regions where more uniform and a lower rate of corrosion is taking place.

The final regime of FFC is termed stage III and is shown by the macroscopic image in Fig. 1d. For stages II and III, the impedance spectra were similar in nature with the loss of the distinct oxide film capacitance from stage I and the development of inductive behavior. The corrosion product of stage III transitioned to an optically darker corrosion morphology than that observed in stage II. Moreover, the global R_p measured by EIS typically increased to more than double the minimum values determined for stage II. The darker color and shift in R_p in stage III may suggest a change in the corrosion mechanism after stage II, governed by changes in the exposed alloy surface and solution chemistry. A thicker corrosion product and rougher surface morphology are associated with this stage of corrosion.

Evolution of Localized Corrosion Morphology of AZ31B at OCP

Further characterization of stages II and III is shown in Fig. 2 with supplemental videos available online. In Fig. 2a, a corrosion filament is observed in the bottom left of the micrograph showing streams of H_2 bubbles emanating from around the filament head. This H_2 stream continued in Fig. 2b along with propagation of the corrosion filament. Nevertheless, H_2 evolution at the head of the advancing filament terminated while the filament continued to propagate, as shown in Fig. 2b and c with an 8-s delta. An outline of the prior location of the filament shown in Fig. 2b is placed on the image in Fig. 2c to illustrate advancement of the filament. In this time frame, to the authors' knowledge, this is the first time that an advancing filament has been reported in a video without the presence of a hydrogen stream emanating at the corrosion front. In addition, filament propagation without H_2 streaming from a filament head was observed at higher frequencies when samples were immersed in more dilute NaCl solutions such as 0.1-M and 0.01-M NaCl (link to videos). The lack of H_2 evolution at the front of an advancing filament could stem from the time it takes H_2 gas to build up underneath the intact oxide-hydroxide film of the Mg matrix, followed by the rupture of the film

Evolution of the Corrosion Morphology on AZ31B Tracked Electrochemically and by In Situ Microscopy in Chloride-Containing Media
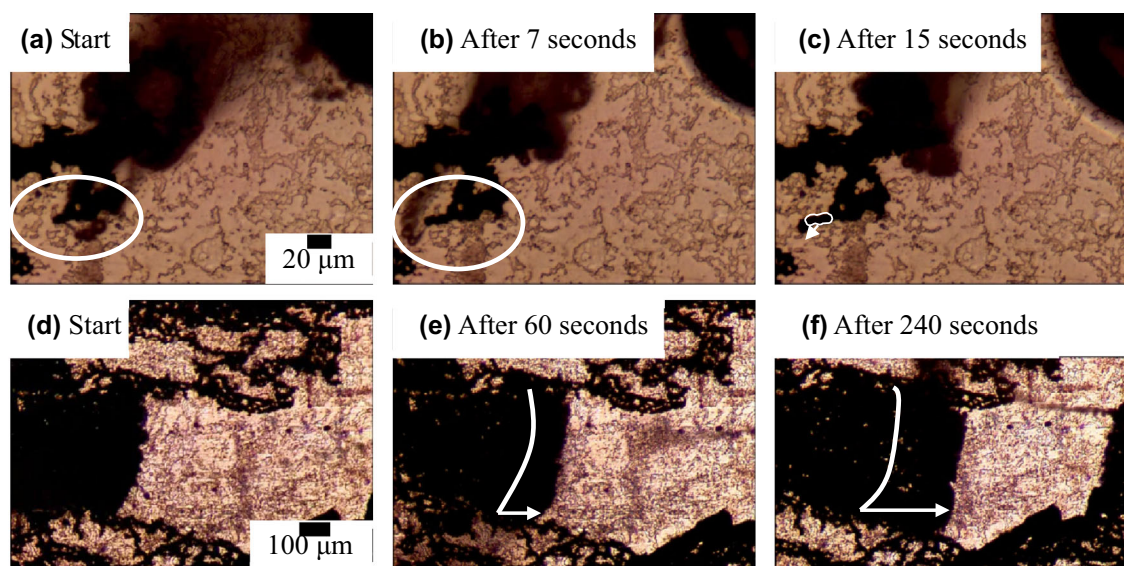
2325

Fig. 2. A time lapse of 15 s for filaments from stage II propagating across the AZ31B specimen, polished to a colloidal finish, after 1 h of immersion in 0.6-M NaCl is shown in (a) to (c). A time lapse of 240 s for a stage III corroding front, propagating across the as-received AZ31B specimen, polished to a colloidal finish, after 5 h of immersion in 0.6-M NaCl is shown in (d) to (f). A supplemental video is available for both sets of images.

and a burst of H_2 gas into the solution. This response would be similar in nature to the rupture of blisters during the pitting corrosion of Al.[28,29] Yet, this burst of H_2 is often not observed when the filament is shown to stop propagation as in Fig. 2. The Mg filament propagation theory put forward by Curioni et al. regarding a "remote anodic current" may explain a filament's ability to shut off without any observable H_2 evolution at the filament head.[10,11] Here a filament has formed a supporting galvanic couple with a cathodic site some distance away from the filament head, leading to an alternative location for H_2 evolution to occur. The lack of H_2 at the filament head would prevent H_2 buildup and the burst of gas to occur, potentially leading to the stopping of filament propagation.

Stage III propagation is shown in Fig. 2d through f where FFCs propagated between the previously corroded filaments from stage II and appear to span the width of previously corroded filaments. The large area covered by the filaments in stage III will be referred to here as a "corrosion front" as they act similar to the radial propagating corrosion fronts observed on low-purity Mg when immersed in higher (> 0.1-M) concentrations of NaCl solutions.[12] This corroding front also accompanied rapid H_2 evolution produced across a more confined area necessitating the use of a lower magnification lens. The appearance of rapid H_2 evolution produced at the corrosion fronts during stage III relative to the shallow filaments of stage II prompted investigation of linear propagation rates for each stage.

Filament Volume Dissolution Rates of AZ31B at OCP

From the videos in Fig. 2 and additional experiments, FFC propagation rates were determined for stages II and III by *ImageJ* analysis. White light interferometry measurements determined the depth of penetration for corrosion filaments. A backscattered SEM micrograph of the surface is shown in Fig. 3a, with stages II and III filaments present. Figure 3b is the corresponding white light interferometry measurement of the area in Fig. 3a, revealing a penetration depth of stages II and III filaments after the specimen was cleaned of the corrosion product. The yellow pixels in the interferometry map were typically observed for the stage III corrosion fronts because of the small sharp features present on the chromic acid cleaned surface.

The propagation rates were determined for individual filaments in stage II. Each filament was found to propagate parallel to the surface at a rate $r_{II} = 1.5 \pm 0.5$ μm/s with an average width of 11 ± 4 μm and depth of 2.6 ± 0.6 μm. For stage III, the FFC propagation rates were determined by measuring the length of each propagating corroding front, which moved across the surface with time, yielding a similar propagation rate in stage III with $r_{III} = 1.5 \pm 0.3$ μm/s with an average FFC depth of 7.3 ± 3 μm. The corroding fronts are similar to the propagation observed for pure Mg when radial corrosion takes place; only these fronts of corrosion activity are bound by the previous FFC filaments from stage II. The width of stage III corroding fronts ranged from several μm to several hundreds of μm as the spacing between stage II filaments dictated their width.
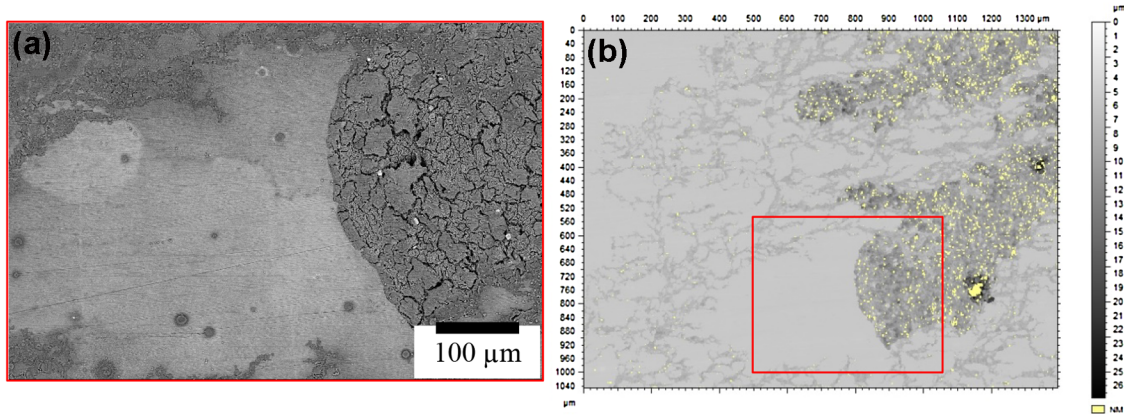
Fig. 3. Backscattered electron micrograph of the as-received AZ31B specimen after 5 h of immersion in 0.6-M NaCl is shown in (a). A white light interferometry topography map of the corresponding area from (a) after chromic acid cleaning is shown in (b), revealing penetration of stage II versus stage III filaments.

The result of this analysis show that a "volume loss" rate of corrosion may be tabulated for stages II and III. In stage II, an average propagation rate of a single filament was 43 μm^3/s. For stage III, a volume loss rate for a broad corroding front was determined with a width of 450 μm and found to be ∼4900 μm^3/s. The width chosen for stage III is from numerous video observations where between one and five corroding fronts were active on the surface after 5 h of immersion, and the combined width of the fronts was approximated at ∼450 μm. From previous work, mass loss over a 24-h period in 0.6-M NaCl was 0.0024 g or 0.6 μm/h.[19,21] Nevertheless, the depth of penetration for filaments far exceeds this upon FFC initiation after 10 min in stage II, at 2.6 μm, and after 5 h, the average penetration was ∼3 μm. In contrast, the penetration depth is greater than 7 μm from interferometry data in stage III. As a result, assuming uniform corrosion of Mg substrates across the entire surface can greatly underestimate the true corrosion depth.

For a single filament in stage II and the corroding fronts of stage III, an R_{FFC} can be estimated using the average linear propagation rate of 1.5 μm/s to be 0.02 Ω-cm^2, assuming the Stern-Geary approach is valid. Using the average propagation rate for each stage did not allow for the discrimination between the two different corrosion morphologies and depths observed. Nevertheless, it is possible to speculate the surface coverage (θ) of active filament area depending on the total global R_p measured by EIS from the equation:

$$\frac{1}{R_p} = \frac{\theta}{R_{FFC}} + \frac{1 - \theta}{R_p^{\text{passive film}}}$$

The θ value is the area of active anodic region associated with all active filaments for stage II or the area of all active corroding fronts in stage III. The $R_p^{\text{passive film}} = 900\,\Omega$ - cm^2 and assumed to be constant at all times. In Table I, the total global R_p

Table I. Overall or global R_p estimated by varying coverage of active corrosion sites

Theta, θ (coverage in cm^2)	Propagation rate estimated global R_p (Ω-cm^2)
0	900
0.00001	621
0.00005	277
0.0001	164
0.0002	90
0.0003	62
1	0.02

is determined by varying θ. This revealed that a surface coverage between 0.0002 and 0.0005 is required to produce a similar decrease in EIS measured R_p as observed in stage II (i.e., from 900 to 200 Ω-cm^2). For stage III, the EIS determined R_p was correlated to a slightly lower θ of around 0.00003. This approach further revealed the actively corroding area, and the low impedance of a few rare active sites dictates the global electrochemical response of a locally corroding Mg surface. At any one time only a very small fraction of the filaments are actively corroding, as supported by the videos, and this could be followed over time. Moreover, it is worth noting that the results were insensitive to plausible variations in the passive film $R_p^{\text{passive film}}$ impedance, suggesting that the surface coverage of the actively corroding area can be accurately assessed when active sites have such a low impedance such as previously observed in the case of Al pitting.[30,31] This analysis is impactful because it indicates that FFC sites propagate at high rates, similar to pitting corrosion in other metals, and that such a small area fraction is active at any one time that a reassessment of cathode area and kinetics is justified. The global EIS measured is the composite impedance of a few active sites propagating at high

Evolution of the Corrosion Morphology on AZ31B Tracked Electrochemically and by In Situ Microscopy in Chloride-Containing Media

2327

rates, whereas the balance of the Mg alloy surface corrodes at a low rate. Nevertheless, the global R_p measured by EIS matches mass loss and H_2 evolution even though it is a composite impedance between two distinctly different sites. The EIS-mass loss-H_2 evolution correlation is not invalid, but the system is far from that of uniform corrosion.

CONCLUSION

As a result of the rapid and violent evolution of hydrogen during the corrosion of AZ31B, careful in situ analysis is an essential element in fully understanding the corrosion mechanism in operation. Through the use of in situ optical microscopy, the ability of corrosion filaments to propagate without the accompaniment of an intense stream of H_2 at the corrosion front has been revealed.

Filament propagation in stages II and III was analyzed given R_{FCC} values obtained from optical microscopy to estimate time-dependent surface coverage values for active sites. The surface coverage of active sites showed a direct influence on the global R_p measured by EIS, with more active filaments, or surface coverage, leading to a lower global value of R_p, clearly observed in the stage II of corrosion.

Regarding engineering application, this work has shown that the application of uniform corrosion models do not apply, as the actual penetration depth is significantly higher at local filaments on the surface, which is analogous to pitting in other materials, e.g., in Al alloys, but extraction of the impedance of local sites, or the active area for a given site impedance are possible with the aid of in situ microscopy. Assumptions of uniform corrosion can greatly underestimate the true penetration depth, which could result in premature mechanical failure.

ACKNOWLEDGEMENTS

ELECTRONIC SUPPLEMENTARY MATERIAL

The online version of this article (doi:10.1007/s11837-017-2377-8) contains supplementary material, which is available to authorized users.

REFERENCES

1. T.B. Abbott, *Corrosion* 71, 120 (2015).
2. J.A. Yuwono, N. Birbilis, K.S. Williams, and N.V. Medhekar, *J. Phys. Chem. C* 120, 26922 (2016).
3. S. Thomas, O. Gharbi, S.H. Salleh, P. Volovitch, K. Ogle, and N. Birbilis, *Electrochim. Acta* 210, 271 (2016).
4. Y. Yang, F. Scenini, and M. Curioni, *Electrochim. Acta* 198, 174 (2016).
5. Z.P. Cano, M. Danaie, J.R. Kish, J.R. McDermid, G.A. Botton, and G. Williams, *Corrosion* 71, 146 (2015).
6. Z.P. Cano, J.R. Kish, and J.R. McDermid, *Magnesium Technology 2014*, ed. M. Alderman, M.V. Manuel, N. Hort, and N.R. Neelameggham (Warrendale, PA: The Minerals, Metals & Materials Society; Hoboken, NJ: John Wiley & Sons, 2014), pp. 335–340.
7. Z.P. Cano, J.R. Kish, and J.R. McDermid, *J. Electrochem. Soc.* 163, C62 (2015).
8. S. Pawar, X. Zhou, G.E. Thompson, G. Scamans, and Z. Fan, *J. Electrochem. Soc.* 162, C442 (2015).
9. L. Yang, X. Zhou, M. Curioni, S. Pawar, H. Liu, Z. Fan, G. Scamans, and G. Thompson, *J. Electrochem. Soc.* 162, C362 (2015).
10. M. Curioni, F. Scenini, T. Monetta, and F. Bellucci, *Electrochim. Acta* 166, 372 (2015).
11. M. Curioni, J.M. Torrescano-Alvarez, Y.F. Yang, and F. Scenini, *Corrosion* 73, 463 (2017).
12. G. Williams, N. Birbilis, and H.N. McMurray, *Faraday Discuss.* 180, 313 (2015).
13. H.M. Krebs, A. Chirazi, L. Lechner, J. Gleb, X. Zhou, G.E. Thompson, and P.J. Withers, "Time-Evolved Correlative Imaging Applied to the Corrosion Study of Mg Alloys In Alkali Environment" (Paper presented at FIMPART 2015, Hyderabad, India).
14. G. Williams, H.L. Dafydd, and R. Grace, *Electrochim. Acta* 109, 489 (2013).
15. G. Williams and R. Grace, *Electrochim. Acta* 56, 1894 (2011).
16. P. Schmutz, V. Guillaumin, R.S. Lillard, J.A. Lillard, and G.S. Frankel, *J. Electrochem. Soc.* 150, B99 (2003).
17. J.M.C. Mol, B.R.W. Hinton, D.H. Van Der Weijde, J.H.W. De Wit, and S. Van Der Zwaag, *J. Mater. Sci.* 35, 1629 (2000).
18. O. Lunder, J.E. Lein, S.M. Hesjevik, T.K. Aune, and K. Nisancioglu, *Werkst. Korros.* 45, 331 (1994).
19. L.G. Bland, A.D. King, N. Birbilis, and J.R. Scully, *Corrosion* 71, 128 (2015).
20. A.D. King, N. Birbilis, and J.R. Scully, *Electrochim. Acta* 121, 394 (2014).
21. M.A. Melia, P. Steiner, N. Birbilis, J.M. Fitz-Gerald, and J.R. Scully, *Corrosion* 72, 95 (2015).
22. M.L. Bland, M.L. Scully, and D.J. Scully, *Corrosion* 0, null.
23. A.S. G1, in, ASTM International, West Conshohocken, PA, 2011.
24. V. Shkirskiy, A.D. King, O. Gharbi, P. Volovitch, J.R. Scully, K. Ogle, and N. Birbilis, *Eur. J. Chem. Phys. Phys. Chem.* 16, 536 (2015).
25. L. Wang, T. Shinohara, B.-P. Zhang, and H. Iwai, *J. Alloys Compd.* 485, 747 (2009).
26. M.P. Brady, G. Rother, L.M. Anovitz, K.C. Littrell, K.A. Unocic, H.H. Elsentriecy, G.L. Song, J.K. Thomson, N.C. Gallego, and B. Davis, *J. Electrochem. Soc.* 162, C140 (2015).
27. K.A. Unocic, H.H. Elsentriecy, M.P. Brady, H.M. Meyer, G.L. Song, M. Fayek, R.A. Meisner, and B. Davis, *J. Electrochem. Soc.* 161, C302 (2014).
28. R.L. Ryan and E. McCafferty, *J. Electrochem. Soc.* 142, 2594 (1995).
29. P.M. Natishan and E. McCafferty, *J. Electrochem. Soc.* 136, 53 (1989).
30. J.R. Scully, D.E. Peebles, A.D. Romig, D.R. Frear, and C.R. Hills, *Metall. Trans. A* 23, 2641 (1992).
31. J.R. Scully, R.P. Frankenthal, K.J. Hanson, D.J. Siconolfi, and J.D. Sinclair, *J. Electrochem. Soc.* 137, 1365 (1990).